

C. KOBER¹ B. ERDMANN C. HELLMICH
R. SADER H.-F. ZEILHOFER

Anisotropic Simulation of the Human Mandible

¹Extended version of a contribution to the 17th ASCE Engineering Mechanics Conference, June 13-16, 2004, University of Delaware, Newark, USA

Anisotropic Simulation of the Human Mandible

Cornelia Kober^{1,5} Bodo Erdmann² Christian Hellmich³
Robert Sader^{4,5} Hans-Florian Zeilhofer^{4,5}

Abstract

We focus on the role of anisotropic elasticity in the simulation of the load distribution in a human mandible due to a lateral bite on the leftmost premolar. Based on experimental evidence, we adopt “local” orthotropy of the elastic properties of the bone tissue. Since the trajectories of anisotropic elasticity are not accessible from Computer Tomographic (CT) data, they will be reconstructed from (i) the organ’s geometry and (ii) from coherent structures which can be recognized from the spatial distribution of the CT values.

A sensitivity analysis comprising various 3D FE simulations reveals the relevance of elastic anisotropy for the load carrying behavior of a human mandible: Comparison of the load distributions in isotropic and anisotropic simulations indicates that anisotropy seems to “spare” the mandible from loading. Moreover, a maximum degree of anisotropy leads to kind of an load minimization of the mandible, expressed by a minimum of different norms of local strain, evaluated throughout the organ. Thus, we may suggest that anisotropy is not only relevant, but also in some sense “optimal”.

1 Introduction

During lifetime, the human mandible is subjected to severe changes, see Figure 1. Due to the loss of the chewing capability, the mechanical stimulus

¹Fac. of Engineering and Computer Science, Univ. of Appl. Sc. Osnabrück, Germany

²Zuse Institute Berlin, Germany

³Institute for Strength of Materials, Vienna University of Technology, Austria

⁴University Hospital Basle, Switzerland

⁵Center of Adv. Studies in Cranio-Maxillo-Facial Surgery, Munich Univ. of Techn., Germany

necessary for the self-regulation of the bony structure vanishes. The shape of the mandibular corpus flattens, while the mandibular angle increases. Because of the interdependence of the inner structure of bone and its functional loading, a refined understanding of the structural behaviour of the jaw is of immediate medical interest.

Three dimensional simulation of the human mandible by means of finite element method started in the early nineties of the last century. Among the pioneers were Koriath et al. [10] and Hart et al. [6]. Both already included material anisotropy into their simulation concept. In the meantime, a rich body of literature is available. As an example of a recent study of anisotropic simulation, we refer to O'Mahony et al. [12].

The work presented in this article is part of an interdisciplinary research project concerning the human mandible with the long-term goal to establish bony organ simulation as a powerful tool for craniofacial or orthodontic therapy. For results, see Kober et al. [9] for instance.

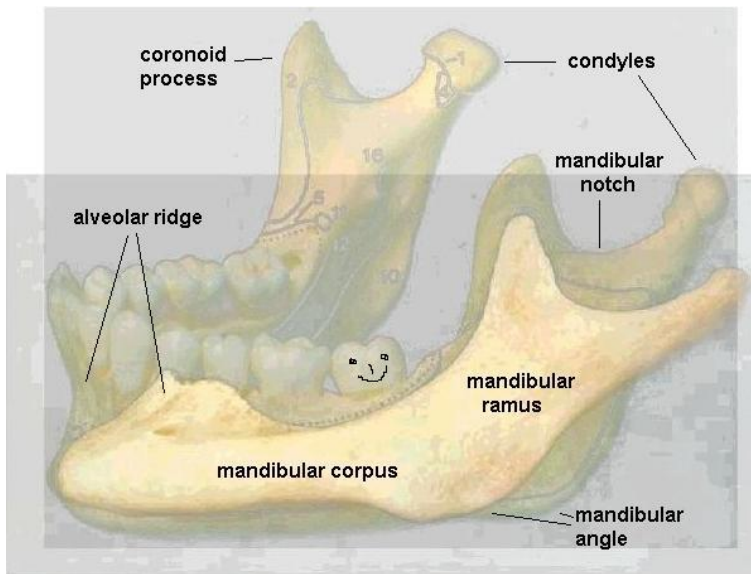


Figure 1: Human mandible at old age and at adulthood (in the background).

2 The Simulation Concept

2.1 Material Law and Finite Element Approximation

Up to a strain limit of 0.3 %, the material behaviour of bone can be described by linear elasticity. In most physiological standard situations, this value is not exceeded. Therefore, in the governing equation of structural mechanics

$$\operatorname{div} \sigma = 0, \quad (1)$$

we apply for the stress tensor $\sigma := (\sigma_{ij})$ and the strain tensor $\varepsilon := (\varepsilon_{ij}) = (\nabla u + (\nabla u)^T)/2$ a generalized Hooke's law which can be written in standard index notation as

$$\sigma_{ij} = C_{ijkl} \varepsilon_{kl}, \quad (2)$$

completed by boundary values. u denotes the displacement vector.

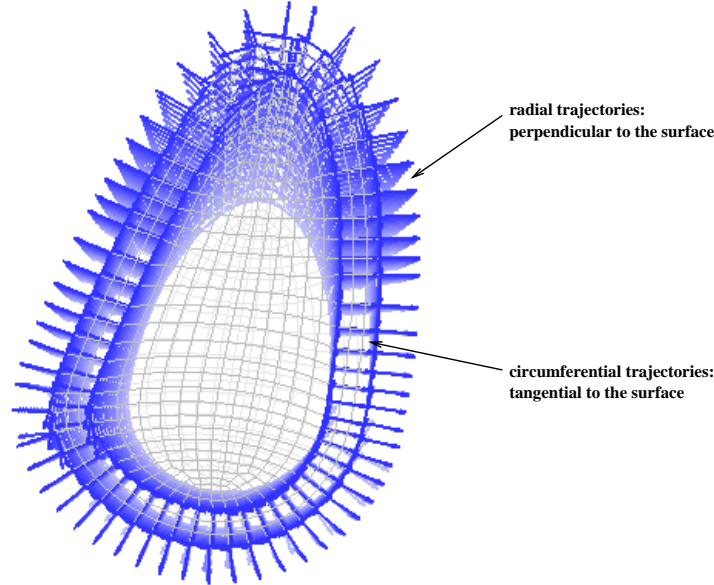


Figure 2: Sketch of a cross section through the mandible with trajectories of elasticity.

Motivated by experimental evidence, e.g. Ashman et al. [1], we consider orthotropic symmetry for the bony tissue. The mechanical properties of orthotropic materials are different in three perpendicular directions. For the mandible, we construct radial, tangential, and axial trajectories, defining the principal orthotropic material directions at each location within the organ, from the irregular organ geometry, see also Figure 2.

In the orthotropic case the relation between stress and strain tensor can be written in the following form

$$\begin{pmatrix} \sigma_{11} \\ \sigma_{22} \\ \sigma_{33} \\ \sigma_{12} \\ \sigma_{13} \\ \sigma_{23} \end{pmatrix} = \mathcal{C} \begin{pmatrix} \varepsilon_{11} \\ \varepsilon_{22} \\ \varepsilon_{33} \\ 2\varepsilon_{12} \\ 2\varepsilon_{13} \\ 2\varepsilon_{23} \end{pmatrix} \quad (3)$$

with the symmetric matrix of elastic coefficients

$$\mathcal{C} = \begin{pmatrix} C_{11} & C_{12} & C_{13} & 0 & 0 & 0 \\ C_{21} & C_{22} & C_{23} & 0 & 0 & 0 \\ C_{31} & C_{32} & C_{33} & 0 & 0 & 0 \\ 0 & 0 & 0 & C_{44} & 0 & 0 \\ 0 & 0 & 0 & 0 & C_{55} & 0 \\ 0 & 0 & 0 & 0 & 0 & C_{66} \end{pmatrix}$$

The relationship (compare [13]) between the coefficients C_{ij} , the Young moduli E_i , the Poisson numbers ν_{ij} and the shear moduli G_{ij} , $i, j = 1, 2, 3$, is given by

$$\begin{aligned} C_{11} &= E_1(1 - (E_3/E_2)\nu_{23}^2)D \\ C_{22} &= E_2(1 - (E_3/E_1)\nu_{13}^2)D \\ C_{33} &= E_3(1 - (E_2/E_1)\nu_{12}^2)D \\ C_{12} &= C_{21} = (E_2\nu_{12} + E_3\nu_{13}\nu_{23})D \end{aligned}$$

$$\begin{aligned}
C_{13} &= C_{31} = E_3(\nu_{12}\nu_{23} + \nu_{13})D \\
C_{23} &= C_{32} = (E_3/E_1)(E_1\nu_{23} + E_2\nu_{12}\nu_{13})D \\
C_{44} &= G_{23} \\
C_{55} &= G_{13} \\
C_{66} &= G_{12} \\
\nu_{ij} &= \nu_{ji}(E_i/E_j) \\
D^{-1} &= 1 - 2(E_3/E_1)\nu_{12}\nu_{23}\nu_{13} - \nu_{13}^2(E_3/E_1) - \nu_{23}^2(E_3/E_2) - \nu_{12}^2(E_2/E_1)
\end{aligned}$$

For the numerical calculations, we have to transform the components of the orthotropic elasticity tensors from the local coordinate system defined by the trajectories to the organ's global coordinate system. Thereby, we have to consider 21 non-zero components instead of nine (independent) non-zero components defined on the local base:

$$\mathcal{C} = \begin{pmatrix} C_{11} & C_{12} & C_{13} & C_{14} & C_{15} & C_{16} \\ C_{12} & C_{22} & C_{23} & C_{24} & C_{25} & C_{26} \\ C_{13} & C_{23} & C_{33} & C_{34} & C_{35} & C_{36} \\ C_{14} & C_{24} & C_{34} & C_{44} & C_{45} & C_{46} \\ C_{15} & C_{25} & C_{35} & C_{45} & C_{55} & C_{56} \\ C_{16} & C_{26} & C_{36} & C_{46} & C_{56} & C_{66} \end{pmatrix}$$

The system of partial differential equations (1) is approximately solved by the adaptive finite element code KASKADE [17, 3, 2, 4]. We used linear elements based on a tetrahedral mesh of the mandible and refrained at the moment from the application of adaptive grid refinement. But, from former studies on the isotropic mandible ([5],[9]) and the high resolution (about 181.000 tetrahedra) of the initial mesh, we may expect that our anisotropic results are qualitatively correct. More accurate calculations using adaptive mesh refinement will follow in the near future.

The field of stiffness tensors \mathbf{C} contains the entire information about tissue anisotropy and organ inhomogeneity. The latter is in some sense “directly” accessible via the information about (optical) density inherent to the data from Computer Tomography (CT). This is not the case for the trajectories of elasticity, which we will estimate from an alternative concept, given in the following subsection. In the next but one subsection, we describe a scenario for testing the influence of the anisotropy. Since we focus on the impact of the tissue anisotropy on the simulation results rather than on the impact of the organ's inhomogeneity, we keep the orthotropic elastic componets constant

over the mandible, differentiating only between cortical and spongy bone, see Table 1. An average ratio of stiffness values of cortical and cancellous bone is about 10:1. Therefore, we set the Young’s and shear moduli of the spongy bone to a tenth of the coefficients cited in Table 1.

E_1	E_2	E_3	ν_{12}	ν_{13}	ν_{23}	G_{12}	G_{13}	G_{23}
10.8 GPa	13.3 GPa	19.4 GPa	0.309	0.381	0.249	3.81 GPa	4.12 GPa	4.63 GPa

Table 1: Elastic coefficients for cortical human jaw bone (Ashman et al., 1987). The 1-direction is radial, the 2-direction is circumferential, and the 3-direction is axial.

2.2 Estimated Trajectories of Orthotropic Elasticity

The collagen molecules are probable to induce a certain morphology in the bone ultrastructure (Hellmich and Ulm [8]) and beyond. On the other hand, they induce the bone tissues’ anisotropy (Lees et al. [11], Hellmich and Ulm [7]). Therefore, we here start the estimation of the trajectories of orthotropic elasticity throughout the organ from (i) the organ’s geometry and (ii) from coherent structures which can be recognized in a volumetric profile of the distribution of the CT or Hounsfield values, see Figure 3. In a four-step procedure (which is only roughly sketched in the following), we construct unit vector fields for the trajectories of elasticity.

Step 1: derivation of an individual inner skeleton of the mandible

For this purpose, we orientated ourselves basically on the patient’s individual anatomy, given by the alveolar ridge, the coronoid processes, and the condyles, see Figure 1. The volumetric profile of the (optical) tissue density depicted in Figure 3 is based on highly transparent modified volume rendering of the CT-data. The condyles are skipped in the visualization because of their reduced Hounsfield values. The (white) “lines of the skeleton” follow mainly the “lines” of elevated Hounsfield numbers (red color in Figure 3). Additionally, we put a line in the middle of the mandibular ramus, in order to represent a “band” of reduced density.

In our rather rough skeleton representation, we neglect a very special formation around the symphyseal line at the chin, where the mandible did coalesce during development, or kind of “reinforcements” at the mandibular notch. Further, we refrained from the reconstruction of the complicated

dental anatomy. For a more refined discussion, see Kober et al. [9].

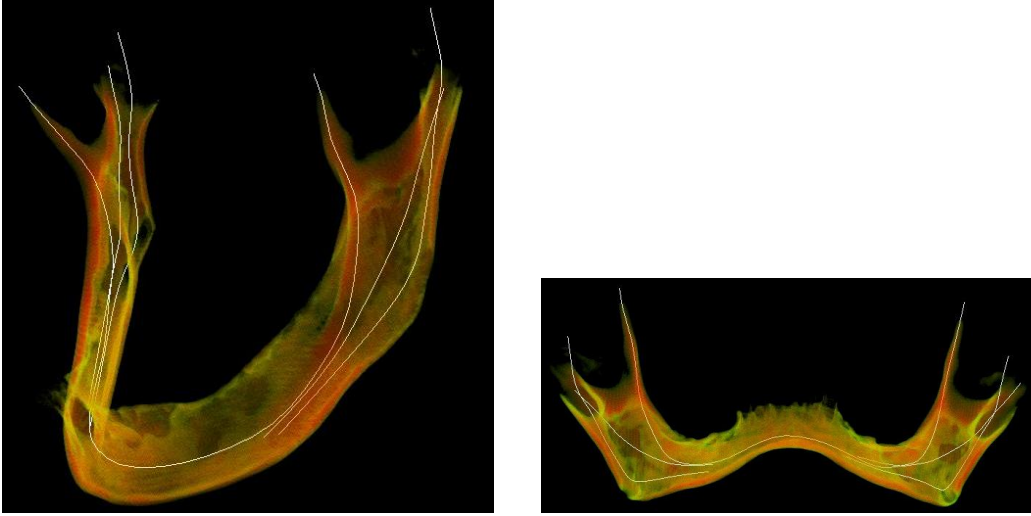


Figure 3: Highly transparent visualization of the inner structure of the cortical shell of a human mandible together with its “inner skeleton”.

Step 2: extension of the skeleton to (nearly) continuous three dimensional vector field

Principally, this extension consists in a nearest-neighbour-interpolation of the skeleton to the whole mandible. Due to the bifurcation at the mandibular ramus, we have to introduce a special interpolation procedure. From a topological point of view, we cannot “comb” the mandible. In the critical bifurcation regions, we seek for the points with minimal distance at the three branches of the skeleton. Now, we claim that every point “insulates” a hemispherical region. The points not insulated by another point are admitted to a linear interpolation. By this, we forbid that the skeleton’s orientation at the posterior part of the ramus has some influence on the vector field at its anterior part and vice versa.

Step 3: construction of the radial trajectories

For this purpose, we modified a surface mesh of the mandible. We removed those parts of the surface mesh whose surface normals deviate from the suggested radial trajectories, see Figure 2.

These are mainly the alveolus and the exits of the mandibular canals. For the construction of the radial trajectories, the surface normals of the remaining surface mesh were projected into the mandible by a nearest point search.

Step 4: construction of the circumferential and the axial trajectories

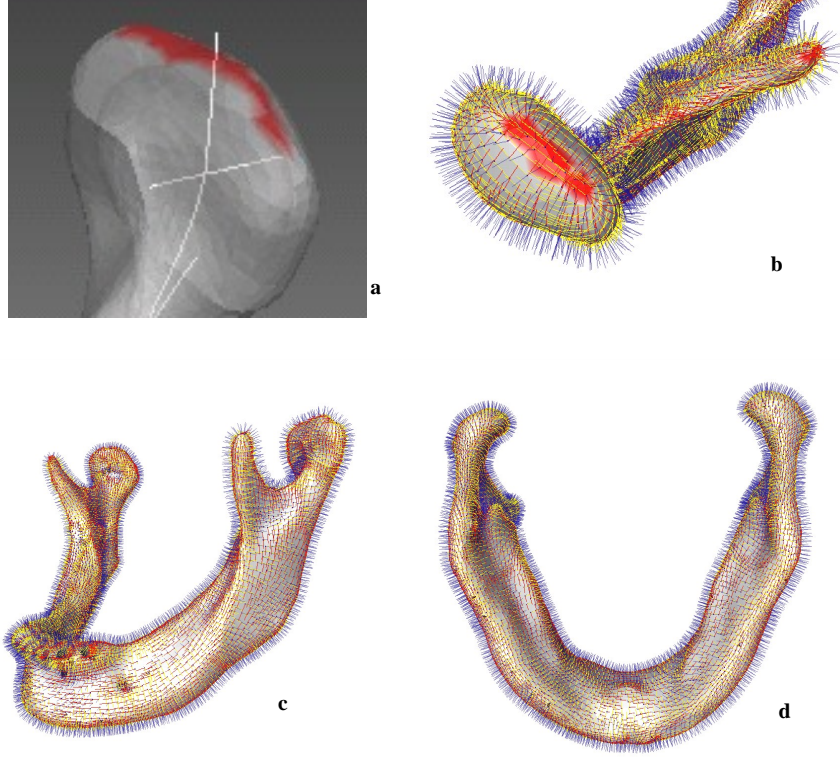


Figure 4: Correction at the condyle (a) and trajectories of elasticity (b c, d; red: axial, yellow: circumferential, blue: radial).

The circumferential trajectories are mainly based on the cross product of the radial trajectories and the “skeleton vectors” of the Step 2. At the top of the condyles and the coronoid processes, and at the mandibular notch, the angle between these vectors becomes very small, see the red marks in Figure 4a, 4b. There, we added a perpendicular correction whose cross product with the radial trajectories allows a (nearly) continuous calculation of the circumferential trajectories, see Figure 4a. The cross product of the circumferential and the radial trajectories produced the axial trajectories. Finally, all three vector fields are scaled to unit vectors. For the result, see Figure 4b, 4c, 4d.

2.3 Scenario for testing the influence of tissue anisotropy on the organ’s load bearing behavior

As in Müller-Hannemann et al. [14], we introduced an index of anisotropy α varying from isotropic material with a low Young modulus over fully

anisotropic behaviour again to isotropic material but with a high Young modulus, see Table 2. We evaluated the cases with $\alpha = 0, 0.25, 0.5, 0.75, 1.0, 1.25, 1.5, 1.75, 2.0$. We tested a lateral bite on the most left premolar. In this load case, the tooth was pressed by the forces of the masticatory muscles against some very hard obstacle. The “biting tooth” was fixed. The condyles were embedded into simplified joint capsules where they were freely mobile. For details, see Kober et al. [9].

Because of its beginning atrophy of the alveolar ridge, we chose the mandible of the female Visible Human as simulation example [15].

	$\alpha = 0$ isotr.	$0 < \alpha < 1$ increas. anisotr.	$\alpha = 1$ anisotr.	$1 < \alpha < 2$ decreasing anisotr.	$\alpha = 2$ isotr.
$E_1(\alpha)$	E_1	E_1	E_1	$E_1 + (\alpha - 1)(E_3 - E_1)$	E_3
$E_2(\alpha)$	E_1	$E_1 + \alpha(E_2 - E_1)$	E_2	$E_2 + (\alpha - 1)(E_3 - E_2)$	E_3
$E_3(\alpha)$	E_1	$E_1 + \alpha(E_3 - E_1)$	E_3	E_3	E_3
$\nu_{ij}(\alpha)$	ν_s	$\nu_s + \alpha(\nu_{ij} - \nu_s)$	ν_{ij}	$\nu_{ij} + (\alpha - 1)(\nu_h - \nu_{ij})$	ν_h
$G_{12}(\alpha)$	G_s	$G_s + \alpha(G_{12} - G_s)$	G_{12}	$G_{12} + (\alpha - 1)(G_h - G_{12})$	G_h
$G_{13}(\alpha)$	G_s	$G_s + \alpha(G_{13} - G_s)$	G_{13}	$G_{13} + (\alpha - 1)(G_h - G_{13})$	G_h
$G_{23}(\alpha)$	G_s	$G_s + \alpha(G_{23} - G_s)$	G_{23}	$G_{23} + (\alpha - 1)(G_h - G_{23})$	G_h

Table 2: Index of anisotropy according to Müller-Hannemann et al. [14]. $\nu_s = \max(\nu_{ij})$, $G_s = E_1/2(1 + \nu_s)$, $\nu_h = \min(\nu_{ij})$, $G_h = E_3/2(1 + \nu_h)$, $1 \leq i, j \leq 3$

3 The Simulation Results

Because of its significance in bone remodeling, we first discuss the results concerning the volumetric strain ε which is the divergence of the strain tensor ε_{ij} , see Figure 5a, 5b, 5c. We observe reduced strain for the anisotropic case (Figure 5b) as well compared to the “soft” mandible in Figure 5a as to the “hard” mandible in Figure 5c. In particular, this effect can be stated at the balancing (right hand) side, but also at both coronoid processes. We may suggest that anisotropy protects the mandible from elevated strain und also endorses unsymmetric loading.

The next question is a quantitative comparison of the results. We look at cortical and spongy bone separately. Because of its special significance,

we differ also between compression and (positive) strain:

$$\varepsilon_{cortical,+} := \max(\varepsilon_{cortical}, 0), \varepsilon_{cortical,-} := \min(\varepsilon_{cortical}, 0) \quad (4)$$

$$\varepsilon_{spong,+} := \max(\varepsilon_{spong}, 0), \varepsilon_{spong,-} := \min(\varepsilon_{spong}, 0) \quad (5)$$

For a first attempt, we compared the L_0 -norms which are maxima of the absolute values of the variables. By elevating the index of anisotropy α , we were stepwise “hardening” the mandible. Spontaneously, one would expect monotonously decreasing strain response. This is true for the spongy variables $\varepsilon_{spong,+}$, $\varepsilon_{spong,-}$, and $\varepsilon_{cortical,+}$, see Figure 6a. But for the L_0 -norm of the compressive strain $\varepsilon_{cortical,-}$ in cortical bone, we have a minimum for the fully anisotropic case indicating that this case is the most “sparing” one concerning compression. Therefore, we extended our analysis to the L_2 -norms which are a measure over the whole mandible:

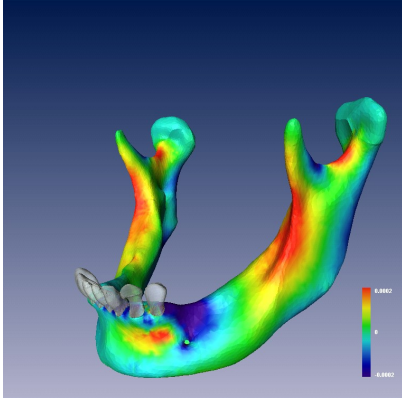
$$\|\varepsilon_{cortical}\| = \sqrt{\int (\varepsilon_{cortical})^2 dx} \quad (6)$$

For the results for $\varepsilon_{cortical}$, $\varepsilon_{cortical,+}$, and $\varepsilon_{cortical,-}$ see Figure 6b. Again, the fully anisotropic cases provide the minima. The results for the spongy bone are reported in Figure 6c. There, no remarkable minima occur for the anisotropic case.

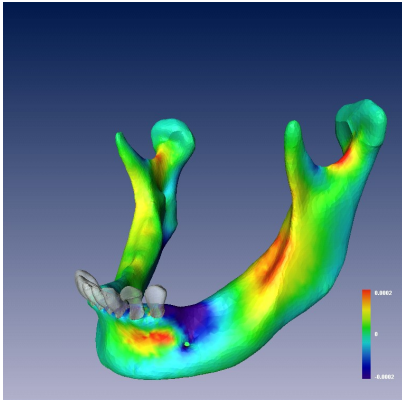
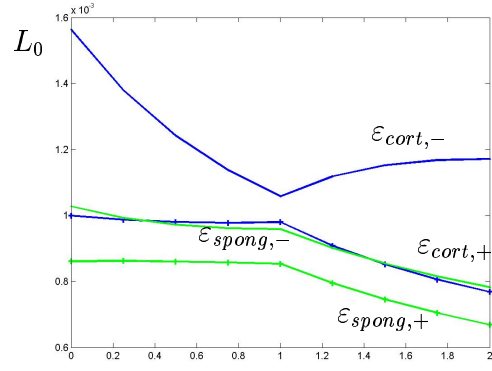
4 Conclusion

The reported test cases suggest qualitative relevance of material anisotropy concerning the simulation of human biting. Especially for volumetric strain, reduced values could be observed, see Figure 5a, 5b, 5c. Further, the asymmetry of the load case was endorsed in the case of anisotropic simulation. Qualitatively, one may reason that anisotropy “spares” the jaw bone from loading.

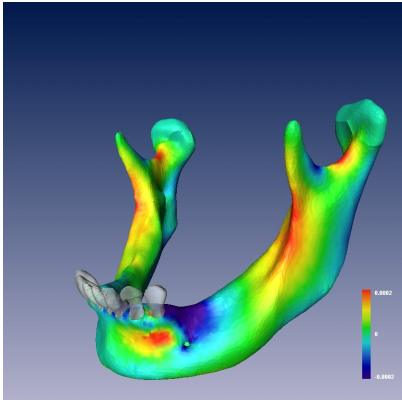
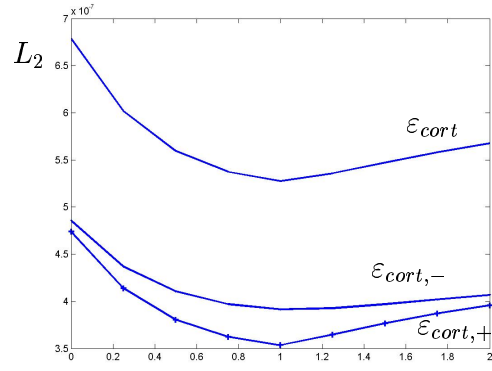
Quantitatively, we achieved even some kind of optimality for the anisotropic case in the sense of minimization of different strain norms. In spite of severe simplifications within our simulation concept, we could reproduce some kind of “mechanical optimality of the mandible”. This fact underlines the necessity of anisotropic simulation for the human mandible, the relevance of our estimation of trajectories of orthotropic elasticity.



a



b



c

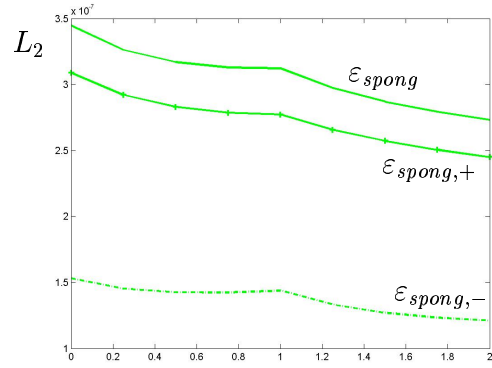


Figure 5: Volumetric strain ε :
a: $\alpha=0$, isotropic, low Young mod.
b: $\alpha=1$, fully anisotropic
c: $\alpha=2$, isotropic, high Young mod.

Figure 6: Norms of ε :
a: L_0 -norm of $\varepsilon_{cort,+}$, $\varepsilon_{cort,-}$, $\varepsilon_{spong,-}$
b: L_2 -norm of ε_{cort} , $\varepsilon_{cort,+}$, $\varepsilon_{cort,-}$
c: L_2 -norm of ε_{spong} , $\varepsilon_{spong,+}$, $\varepsilon_{spong,-}$

5 Acknowledgement

The first author wants to acknowledge H.-C. Hege and his team at ZIB Berlin for the good cooperation and the Amira license. All visualizations besides the diagrams are performed with Amira 3.1 (see [16]). Further, the authors want to thank Götz Bock, Munich Univ.of Techn., for his continuous help, especially concerning the network. Last not least, we are grateful for the computational assistance by Rainer Roitzsch, ZIB Berlin.

References

- [1] R.B. Ashman and W.C. Van Buskirk: Elastic Properties of a Human Mandible, *Adv. Dent. Res.*, 1 (1987), pp. 64-67.
- [2] F. Bornemann, B. Erdmann, R. Kornhuber: Adaptive multilevel-methods in three space dimensions, *Int. J. Num. Meth.in Eng*, Vol. 36 (1993), pp. 3187-3203.
- [3] P. Deuffhard, P. Leinen, H. Yserentant: Concepts of an Adaptive Hierarchical Finite Element Code. *IMPACT Comp. Sci. Eng.* 1 (1989), pp. 3-35.
- [4] B. Erdmann, J. Lang, R. Roitzsch: KASKADE–Manual, Technical Report TR 93-05, Konrad–Zuse–Zentrum Berlin (ZIB), 1993.
- [5] B. Erdmann, C. Kober, J. Lang, P. Deuffhard, H.-F. Zeilhofer, R. Sader: Efficient and Reliable Finite Element Methods for Simulation of the Human Mandible, *Proceedings of 9th Workshop on The Finite Element Method in Biomedical Engineering, Biomechanics and Related Fields*, CDRom, Ulm, Germany, July 2002.
- [6] R.T. Hart, V.V. Hennebel, N. Thongpreda, W.C. van Buskirk, and R.C. Anderson: Modeling the Biomechanics of the Mandible: A Three-Dimensional Finite Element Study, *J. Biomechanics*, 25 (1992), pp. 261-286.
- [7] C. Hellmich and F.-J. Ulm: Are mineralized tissues open crystal foams reinforced by crosslinked collagen? Some energy arguments, *J. Biomechanics.*, 35 (2002), pp. 1199-1212.
- [8] C. Hellmich and F.-J. Ulm: Average hydroxyapatite concentration is uniform in the extracollagenous ultrastructure of mineralized tissues:

- evidence at the 1 - 10 microns scale, *Biomech. Model Mechanobiol.*, 2 (2003), pp. 21-36.
- [9] C. Kober, B. Erdmann, R. Sader, and H.F. Zeilhofer: Simulation (FEM) of the human mandible: a comparison of bone mineral density and stress/strain profiles due to the masticatory system, *Proceedings 10th Workshop, "The Finite Element Method in Biomedical Engineering, Biomechanics and Related Fields"*, Ulm, Germany, July 17-18, 2003.
 - [10] T.W. Koriath, D.P. Romilly, and A.G. Hannam: Three Dimensional Finite Element Stress Analysis of the Dentate Human Mandible, *Am. J. of Phys. Anthr.*, 88 (1992), pp. 69-96.
 - [11] S. Lees, J. Heeley, and P. Cleary: A study of some properties of a sample of bovine cortical bone using ultrasound, *Calcified Tissue International*, 29 (1979), pp. 107-117.
 - [12] A.M. O'Mahony, J.L. Willimans, and P. Spencer: Anisotropic elasticity of cortical and cancellous bone in the posterior mandible increases peri-implant stress and strain under oblique loading, *Clin. Oral Impl. Res.*, 12 (2001), pp. 648-657.
 - [13] R.L. McCullough: Introduction to anisotropic elasticity. In: L.A. Carlson, J.W. Gillespie, editors, *Delaware composites design encyclopedia*, Vol.2 (1990), Lancaster (PA) USA, Technomic Publishers Co..
 - [14] M. Müller-Hannemann, C. Kober, R. Sader, and H.-F. Zeilhofer: Anisotropic Validation of Hexahedral Meshes for Composite Materials in Biomechanics, *Proceedings of the 10th International Meshing Roundtable*, Newport Beach, USA, Oct 10-13, 2001, pp. 249-260.
 - [15] National Library of Medicine. The Visible Human Project, http://www.nlm.nih.gov/research/visible/visible_human.html, 1995.
 - [16] D. Stalling, M. Zöckler, H.-C. Hege: AMIRA – Advanced Visualization, Data Analysis and Geometry Reconstruction. <http://amira.zib.de>
 - [17] <http://www.zib.de/SciSoft/kaskade>